AIAA Journal
Vol. 47, No. 12, December 2009

Flap Vortex Management Using Active Gurney Flaps

David Greenblatt*
Technion—Israel Institute of Technology, Haifa 32000, Israel
Stefan Vey† and Oliver C. Paschereit‡
Technical University of Berlin, 10623 Berlin, Germany
and
Robert Meyer§
DLR, German Aerospace Center, 10623 Berlin, Germany

DOI: 10.2514/1.41767

An experimental study was conducted to assess the applicability of limited-span Gurney flaps for altering the flap-edge vortex characteristics of a swept constant-chord half-model with a commercial aircraft airfoil and high-lift system (slat and flap). The strategy employed was based on the well-known vortex roll-up relations between the span loading and the wake that were extended and modified to include configurations with flapped wings. Phase I of the study involved the testing of static Gurney flaps mounted at the trailing edge and flap edge, in which different flap heights and fractions of flap span were evaluated. Data acquisition included particle image velocimetry measurements downstream of the flap edge, six-component load measurements, and surface pressure measurement on the main element and in the flap-edge region. The Gurney flaps produced significant variation of the vortex centroids, up to 5.3% of the semispan (13.1% of chord), with corresponding small changes to lift and drag coefficients. Phase II of the study involved the evaluation of dynamically deployed Gurney flaps, in which phase-averaged particle image velocimetry measurements were made of the vortex trailing the flap. This was motivated by the desire to periodically perturb the vortex centroids, with a view to exciting wake instabilities and thus triggering a faster decay. When driving the Gurney flap and hence perturbing the vortices at wavelengths shorter or longer than the wingspan, the authority over the vortex centroids did not materially change.

Nomenclature

AR	=	aspect ratio
b	=	wingspan
C_D	=	model drag coefficient
C_L	=	model lift coefficient
C_l	=	sectional lift coefficient
C_M	=	model moment coefficient
c	=	model chord length
h_G	=	Gurney flap height relative to the chord
l_G	=	Gurney flap span relative to the flap span
q	=	freestream dynamic pressure
Re	=	Reynolds number based on chord length
r	=	distance measured form the vortex center
U, V, W	=	mean velocities in directions x, y, z
U_∞	=	freestream velocity
x, y, z	=	coordinates measured from model leading edge and root (left-hand system)
$(\bar{y}, \bar{z})$	=	vortex centroid location in the (y, z) plane
α	=	angle of attack
Γ	=	bound circulation
Γ'	=	rolled-up wake vortex strength
γ	=	vortex-sheet strength, $d\Gamma/dy$
δ	=	flap deflection angle
δ_G	=	Gurney flap angle
Λ	=	sweepback angle
λ	=	wavelength
Φ	=	phase shift, deg
ω_x	=	streamwise vorticity, $\partial W/\partial y - \partial V/\partial z$

Subscripts

bl	=	baseline (no control case)
f	=	trailing-edge flap
s	=	semispan

Presented as Paper 0286 at the 46th AIAA Aerospace Sciences Meeting and Exhibit, Reno, NV, 7–10 January 2008; received 23 October 2008; revision received 15 July 2009; accepted for publication 2 September 2009.

*Senior Lecturer, Faculty of Mechanical Engineering; davidg@technion.ac.il. Senior Member AIAA.

†Graduate Student, Chair of Fluid Dynamics, Hermann-Föttinger-Institute, Technical University of Berlin; stefan.vey@pi.tu-berlin.de.

‡Professor, Chair of Fluid Dynamics, Hermann-Föttinger-Institute, Technical University of Berlin; oliver.paschereit@pi.tu-berlin.de. Senior Member AIAA.

§Research Scientist, Engine Acoustics, Institute of Propulsion Technology, Müller-Breslau Strasse 8; robert.meyer@dlr.de.

I. Introduction

THE well-known hazard posed by powerful vortices trailing large commercial airliners (Spalart [1] and Rossow [2]) is particularly severe near airports where planes fly in close proximity and where the relatively low flight speeds result in increased vortex strength. In order to safely avoid wake vortex encounters, interaircraft separation standards are enforced in which larger separation distances are imposed in the wakes of larger airliners. A number of studies have shown that the vortex hazard is a major factor contributing to inefficient throughput and delays at busy modern airports (e.g., [3]). Moreover, with projected increases in the demand for air transportation [3] and ever-larger aircraft entering the fleet mix (Kingsley-Jones [4]), it is expected that the increased hazard will be a significant impediment to future air traffic capacity.

Vortex alleviation techniques, which aim to directly reduce the wake severity by modifying its vortex characteristics, can potentially reduce aircraft-following distances (see Savaş [5], Crouch [6], and [3]). The viability of a vortex alleviation method is quantified by a reduction in the severity and probability of a vortex encounter, and a hazard boundary [3] can be defined that relies on effective wake detection and simulation (e.g., Michel and Böhning [7], Schmitt et al. [8], Fine and Kring [9], and Frech and Holzäpfel [10]). Vortex alleviation techniques employed, however, must not degrade performance or compromise safety and ride quality.

Effective vortex alleviation methods fall into two broad categories: time-invariant and time-dependent methods. The former relies on modifying the span-loading to establish two or more pairs of opposite-signed counter-rotating vortices and allow naturally arising instabilities to bring about their linking and mutual destruction (Rennich and Lele [11], Rossow [12], Cliffone and Orloff [13], Ortega et al. [14], Fabre et al. [15], Durston et al. [16], and Savaş [5]). In many instances, the required configuration modifications adversely affect aircraft performance and this limits their potential implementation [3]. The latter method actively forces the breakup of vortices, for example, by pitching the aircraft (Chevalier [17]) or differentially and time-dependently deflecting inboard and outboard control surfaces (sloshing of the lift distribution) (Crow [18], Crow and Bate [19], and Haverkamp et al. [20]). This method was tested in a towing tank (Bilanin and Widnall [21]), where measured amplification rates agreed qualitatively with theoretical predictions. Recently, a similar approach was pursued with a view to exploiting the multiple vortex growth mechanisms created by an airplane on approach with flaps down (Crouch el al. [22]). Another approach exploits transient growth or bypass mechanisms of the vortex pair (Pradeep and Hussain [23] and Brion et al. [24]). Despite their inherent appeal, active methods must address issues such as "ride quality, dynamic-load effects on the structure, and the ability to maintain control authority during operation" [25].

Recent years have witnessed a different approach to vortex management that effectively decouples wake vortex control from standard control surfaces. Various techniques have been proposed, such as steady blowing from the flap edge (Coustols et al. [26]), the deployment of active Gurney flaps at wingtips (Matalanis and Eaton [27,28] and Nikolic [29]), and passive and active control of boundary-layer separation (Greenblatt [30,31] and Greenblatt et al. [32]). These methods show application potential because they achieve significant authority over vortices with devices that can be retrofitted to wings or flaps. Furthermore, there is evidence that authority over the vortices can be achieved with minimal variation of the wing loads.

II. Flap-Vortex Control Rationale

All modern airliners deploy flaps for takeoff and landing. Thus, in the flight regimes in which the hazard is most severe (namely, low-speed flight in the vicinity of airports), the flap-edge vortex dominates the ensuing wake structure. This is observed in wind-tunnel investigations (de Bruin et al. [33] and Bellastrada et al. [34]) and flight measurements (Donaldson et al. [35]) and is also clearly evident when observing the contrails in cold or humid weather (see the photographs in Figure 1). The pressure drop in the vortices is proportional to the square of the vortex strength, and the accompanying drop in temperature produces the contrails visible in the photographs.

Controlling separation or circulation locally (i.e., over some fraction of the flap span) in the vicinity of the flap edge directly affects lift or bound circulation Γ and therefore modifies the vortex-sheet strength (or shed vorticity) $\gamma = d\Gamma/dy$. Since the vortex sheet at the flap edge rolls up into the dominating vortex, local separation control or manipulation of the local span-loading are strong candidates for directly controlling or managing the vortices. Furthermore, decoupling vortex management from the control surfaces and only applying it selectively ensures relatively small wing-load excursions. The aforementioned assertions were initially made by Greenblatt [30,31] based on the method of Betz [36] as extended by Donaldson et al. [35]. The principle computational advantage of Betz's [36] method is that it does not explicitly treat the roll-up mechanism, but rather employs three conservation relations between the span-loading $\Gamma(y)$ and the rolling-up vortex $\Gamma'(r)$. Betz employed conservation of vorticity and also postulated that the first and second moments of vorticity are conserved: these are referred to as the inviscid roll-up relations. Despite the relative simplicity of the method, it predicts flap-vortex details that are in surprisingly good agreement with full-scale airliner flight tests [35].

The present approach is based on a pilot study conducted at NASA Langley Research Center [31,32], where boundary-layer separation control was used to investigate the concept and viability of near-wake vortex management on a flapped semispan model. Separation control was found to have a marked effect on vortex location, strength, tangential velocity, axial velocity, and size over a wide range of angles of attack and control conditions. In general, the vortex trends were well predicted by the inviscid roll-up relations of Betz [36] and Donaldson [35], and the vortex centroid predictions were excellent. Manipulation of the separated flow near the flap edges exerted significant control over either outboard or inboard edge vortices while producing small lift and moment excursions. Nevertheless, Greenblatt [30,31] did not explicitly address four important factors:

1) The investigation was conducted on a semispan model with simple flaps and not high-lift devices encountered on modern airliners.

2) The model did not incorporate sweep, which is prevalent on all modern airliners.

Fig. 1 Photographs showing condensation in flap-edge vortices. The source of the lower two figures is www.airliners.net. All photographs are reproduced with permission.

3) Wing loads were not explicitly measured, but rather inferred from discrete surface pressure measurements.

4) Only near-field ($x/c = 2$) vortex measurements were made. The present investigation was undertaken with the express purpose of redressing these deficiencies.

III. Objective and Scope

The global objective of the present investigation was to assess the viability of vortex management, by means of local circulation control, within the context of modern airliner configuration. Hence, the investigation was conducted on a swept constant-chord half-model (SCCH) (Fig. 2a) incorporating a modern transonic airfoil of a commercial European airliner and a modern three-element high-lift system. Partial-span Gurney flaps were used for locally altering the span-loading (i.e., vortex-sheet strength) in the vicinity of the flap edge. Full details of the experimental configuration are presented in Sec. IV.

The investigation was divided into two phases: phase I involved the static testing of different finite-flap-span Gurney flap configurations; phase II considered dynamic control of the system (i.e., oscillatory deployment of Gurney flaps). Phase I comprised the major component of the investigation in which vortex properties were estimated from planar particle image velocimetry (PIV) measurements downstream of the model (Sec. V). In addition, surface pressure measurements were made on the flap and main element (Sec. VI), and aerodynamic loads were measured by means of a six-component force-balance (Sec. VII). Phase II involved phase-averaged PIV measurements of the dynamically perturbed vortices, in which specific Gurney flap configurations were selected based on the results of phase I (Sec. VIII). A comparison of different techniques is presented in Sec. IX.

IV. Experimental Configuration

The investigation was conducted on a swept constant-chord half-model (Fig. 2a) incorporating a modern transonic airfoil of a commercial European airliner ($\Lambda = 30$ deg, $b_s = 1.12$ m, $c = 0.45$ m, and $AR = 5$) and a modern three-element high-lift system. The original high-lift system comprised a full-span leading-edge slat and full-span trailing-edge flap (Meyer et al. [37]). For this investigation, the flap was rendered into two equal-span halves (inboard and outboard). The inboard flap and full-length leading-edge slat were set for a typical landing configuration, with a $\delta = 32$ deg flap angle and a 26.5 deg slat angle, whereas the outboard flap was not deflected. Flap and slat settings were achieved by means of brackets located on the wing lower surface. The vast majority of vortex measurements were made with the model at $\alpha = 5$ deg, which is representative of an aircraft on approach for landing, although additional measurements were made at $\alpha = 0$ and 10 deg as a check on the PIV-data consistency.

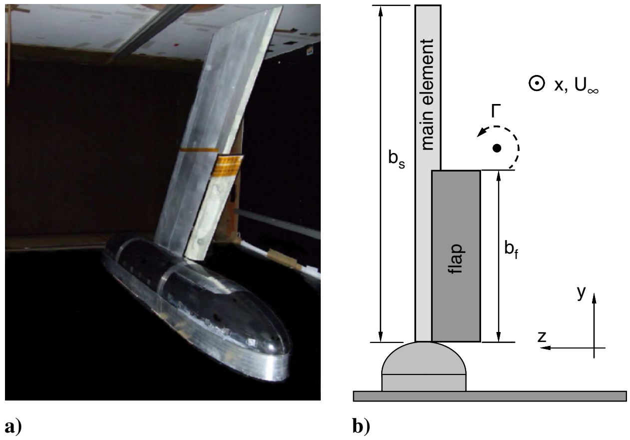

a) b)

Fig. 2 Installation and coordinate system: a) aft photograph of the SCCH used in the experimental study at the Technical University of Berlin, installed in the Institut für Strömungsmechanik und Technische Akustik 2 x 1.41 m closed-loop-return wind tunnel (inboard flap deflected to 32 deg is visible; taped sections indicate locations of main element and flap pressure ports) and b) schematic showing the aft CCD camera view of the setup and coordinate convention.

In contrast to separation control employed in the previous pilot study [31], Gurney flaps were used presently for locally altering the span-loading (i.e., vortex-sheet strength) in the vicinity of the flap edge. These were made from 0.5 mm sheet metal and were fitted to the flap trailing edge. Gurney flap height relative to the chord was designated h_G and Gurney flap length relative to the flap span was designated l_G. The investigation was divided into two phases: phase I involved the static testing of different finite-flap-span Gurney flaps in order to isolate the most promising configurations (see Fig. 3a); phase II employed dynamic control of the system (i.e., oscillatory deployment of Gurney flaps using the configurations isolated in phase I). To achieve this, the Gurney flap was hinged at the flap trailing edge and was driven by pushrod actuation. The pushrod was driven by an electric motor and a cam assembly that was installed in the fuselage of the model. A schematic of the active Gurney flap is shown in Fig. 3b.

For the static case, aerodynamic loads were measured by means of a high-accuracy six-component force balance. Furthermore, the inboard flap was equipped with five rows of pressure ports on the outer 15% of the flap span. The main element incorporated one row of pressure ports corresponding to a location outboard of the flap edge. The balance was designed and built by the company Schenk and has full-scale lift and drag measurement ranges of 3040 N. A direct in-house calibration carried out on the balance, for the range of measurements under consideration, indicated that the errors due to nonlinearity for both lift and drag forces were never greater than 0.23%. Differential pressures on the flap and main element were measured using a Baratron® pressure transducer with a 1000 Pa range and an indicated accuracy of 0.3% full scale.

The wind-tunnel test section was 10 m long, facilitating wake measurements within the range $x/b \leq 4.5$ ($x/c \leq 22$). Rudimentary smoke-based flow visualization was performed of both the flap edge and wingtip vortices. Vortex centroids and strength were estimated from planar two-dimensional PIV measurements at the two downstream locations $x/c = 4$ and 9, corresponding to $x/b = 0.80$ and 1.81, respectively. (The unexpected phenomenon of flap-edge vortex breakdown at $x/c \approx 15$ precluded meaningful measurements further downstream; see the discussion below.) The measurements were made with two Nd:YAG 17 mJ lasers and a 1024×1024 pixel charge-coupled device (CCD) camera. The camera was placed directly behind the flap at $x/c \approx 20$; the camera-view coordinate convention is shown schematically in Fig. 2b and further elucidated in [38]. Two commercial seeding particle generators (Palas AGF 10.0) were used to generate particles of 0.4 μm diameter, based on the manufacturer's specifications, at the downstream end of the test section. Sufficient time was allowed to elapse until the seeding in the test section was homogeneous. Resolution of the PIV images was 0.18 mm/pixel and the particle image size was approximately 2 pixels. Data were processed in 32×32 pixel interrogation areas with 50% overlap. Interrogation areas were cross-correlated and a local median filter was used to eliminate spurious vectors. Spurious

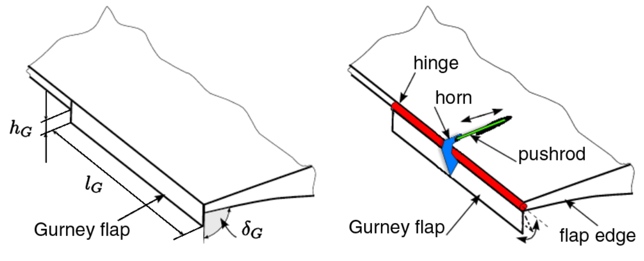

a) b)

Fig. 3 Illustrations of a) static Gurney flap definitions and b) active Gurney flap hinged at the trailing edge of the flap.

vectors were detected by applying a combination of global and local velocity filters. The global filter was used to detect vectors that were outside a user-defined velocity region. The local filter filtered vectors by calculating each vector's deviation from its neighboring vectors. The filtered vectors were then interpolated using the valid surrounding vectors. Nevertheless, the fraction of spurious vectors never exceeded 3% in all of the PIV-data acquired. Various interpolation grid refinements and threshold detection settings were considered, and it was established that none of the parameters had a significant influence on the calculated location of the centroid. Based on these parametric considerations, the maximum error of any calculated centroid was estimated at less than 5%.

V. Static Vortex Measurement

PIV measurements were performed in the wake aft of the inboard flap for a wide variety of configurations. Vorticity fields ω_x with superimposed velocity vectors are shown for several cases in Figs. 4a–4d and indicate the range of movement and strength of the flap-edge vortex ($Re = 500,000$ and $\alpha = 5$ deg). For all cases, the vorticity field was calculated from the average velocity field, based on 300 image pairs, where Gurney flap heights, lengths, and locations were varied to determine the dependence of centroid and vortex strength on the specific configuration. A comparison of Figs. 4a and 4b shows that a Gurney flap mounted on the outboard part of the flap ($h_G = 2\%$ and $l_G = 30\%$) displaces the vortex outboard (toward the wingtip) and slightly upward. It also produces a larger and more diffuse vortex. The outboard displacement results from the fact that the vortex-sheet peak is displaced outboard and this displacement can be quantified by the Donaldson–Betz theory [31,38]. The larger, more diffuse vortex results from the relatively large wake generated by the Gurney flap [37], which is rolled up into the vortex. A further increase in the Gurney flap height ($h_G = 4\%$; Fig. 4c) further diffuses the vortex, but does not displace it significantly more outboard. This indicates qualitatively that the relationship between vortex centroid displacement and h_G is not linear. In the final example, the Gurney flap is moved toward the leading edge by 2% of chord (Fig. 4d). This effectively reduces the displacement of the vortex toward the wing tip. To quantify the changes, vortex strength and centroid were determined by integrating the experimental data using

$$\Gamma = \int \omega_x \mathrm{d}A \qquad (1)$$

and

$$(\bar{y}, \bar{z}) = \frac{1}{\Gamma} \int (y, z) \omega_x \mathrm{d}A \qquad (2)$$

where the integration regions were chosen such that $\omega_x \ll \omega_{x,\max}$ at the boundaries. Centroids calculated using to Eqs. (1) and (2), based on the vorticity fields, such as those illustrated in Figs. 4a–4d, are shown in Fig. 5. The baseline case is indicated by the + symbol; all other symbols represent controlled cases, and the dotted lines joining data points indicate increasing flap length fraction l_G. The figure indicates an apparent optimum in Gurney flap length in terms of spanwise centroid shift for the 2 and 4% Gurney flaps at $l_G = 30\%$ for the $x/c = 4$ position. This observation is consistent with the Donaldson–Betz theory, as changes to local bound circulation near the flap edge have the largest effect on the vortex centroid. As the bound circulation is varied further inboard by the extended Gurney flaps, as expected, this has a diminishing effect on the flap-edge vortex.

As in the example of Fig. 4d, configurations were also tested in which the Gurney flaps were located at 2 and 4% of chord from the trailing edge toward the leading edge. The reason for studying these configurations is because mounting active Gurney flaps at the trailing edge may be difficult practically or may compromise structural integrity. For this reason, similar configurations have been widely studied, and an active version was flight-tested on a modern European airliner (e.g., Hansen [39]). From the data acquired here it can be seen quantitatively that the vortex centroid authority in these cases is reduced when compared to a Gurney flap that is placed flush with the trailing edge. For example, forward movement of the

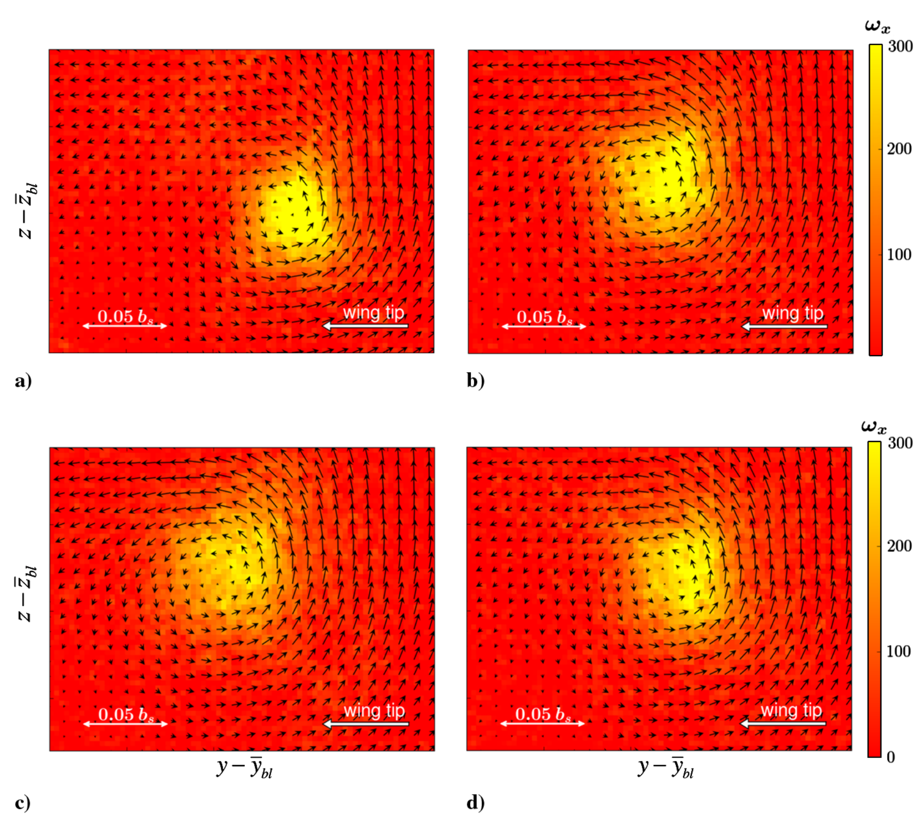

Fig. 4 Vorticity and velocity fields at $x/c = 4$ for a) baseline b) $h_G = 2\%$ and $l_G = 30\%$, c) $h_G = 4\%$ and $l_G = 30\%$, and d) $h_G = 2\%$ and $l_G = 40\%$, 2% from the trailing edge.

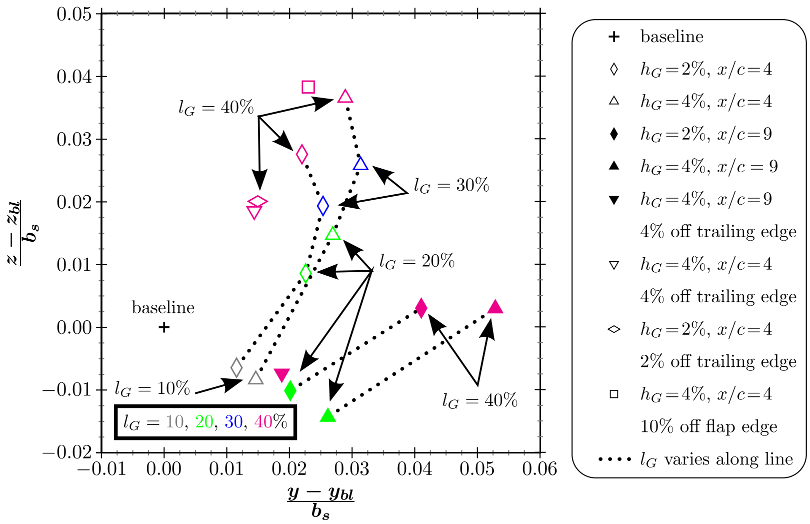

Fig. 5 Centroid shifts (relative to baseline configuration) attained with static Gurney flaps. Dotted lines denote varying Gurney flap length l_G, whereas height h_G is kept constant; $Re = 500,000$ and $\alpha = 5$ deg.

Gurney flap 4% from the trailing edge reduces the centroid displacement by approximately half in both the lateral (spanwise) and longitudinal directions at $x/c = 4$; the authority is further reduced at $x/c = 9$. This result is supported by the findings of Li et al. [40], who varied Gurney flap deflection angle and distance from the trailing edge. They found that Gurney flap efficiency is highly dependent on distance of placement from the trailing edge.

An additional configuration (namely, the displacement of the Gurney laterally inboard of the flap edge toward the root) was also tested. There were two main reasons for considering this configuration. First, on many airliners, the installation of a Gurney flap flush with the flap edge may be impractical or impossible; hence, the testing of the Gurney flap mounted 10% from the flap edge may be representative of a practical configuration. The figure shows that this configuration achieves 80% of the lateral deflection and similar longitudinal deflection as that produced by the flush-mounted Gurney flap. This provides an indication that such a configuration may be both effective and practical in certain instances. The second motivation was related to developing a vortex perturbation scheme in which the Gurney flap slides periodically along the trailing edge. The motivation was to develop a Gurney flap that perturbs the vortex while maintaining constant loads on the aircraft. Here, we consider the change in centroid location between the flush-mounted flap and the flap mounted 10% inboard from the flap edge. As noted above, this only produced a slightly smaller lateral displacement of the centroid than the flush-mounted configuration (i.e., 20%). Hence, the concept of a sliding Gurney flap would require a travel considerably larger than 10% of the flap span in order to achieve comparable authority to that achieved by simply deploying the Gurney flap.

PIV measurements further downstream ($x/c = 9$) revealed that the lateral and longitudinal vortex centroids behaved differently with downstream distance. Lateral displacement increased with downstream distance for both $h_G = 2$ and 4%, but longitudinal displacement tended to zero. Based on theoretical considerations, the vortex further downstream has rolled up more of the vortex sheet and is thus more representative of the changes to the loading on the wing and, in particular, near the flap edge. Flap-edge pressure measurements confirmed the relatively strong local effect of the Gurney flaps in this region, as discussed in the next section.

VI. Flap-Edge Loads

Pressure coefficient distributions were measured in the vicinity of the flap edge for $0.85 < y/b_f < 1$ (Figs. 6a–6e) and on the main element at $y/b_f = 1.05$ (Fig. 6f) for different Gurney flap heights. Based on the pressure transducer uncertainty (see Sec. IV), the pressure coefficient errors are typically less than 1.5% and hence error bars are too small to practically add to the figure. As expected, the Gurney flaps increase the loading on the flap, as can be seen by the lower pressures over the entire flap upper surface. This result is consistent with data acquired on airfoils (Jeffrey et al. [41]) and two-element configurations (Jeffrey et al. [42]). On the flap lower surface, near the trailing edge, the pressure decreases as a result of the Gurney flap. This is contradictory to observations made on unswept multi-element airfoils fitted with Gurney flaps, where the pressure increases toward the flap trailing edge [42]. At present there is no obvious explanation for this, although it is clearly a result of the wing sweepback, which suggests two possible explanations that are not mutually exclusive. One is that the component of velocity tangential to the trailing edge as a result of the Gurney flap produces a low-pressure region; the other is that the combined effect of the sweep and Gurney flap produces a trapped vortex, thereby lowering the pressure. Gurney flaps attached to the flap trailing edge also influence the pressure distribution on the main element up to the leading edge, as shown by the measurement at $y/b_f = 1.05$ (Fig. 6f). The changes are relatively small because the row of pressure ports was located 5% outboard of the flap edge. It is clear that the effect of the Gurney flaps diminished with spanwise distance outboard. Indeed, according to the theory, this must be so, otherwise no changes to the spanwise vortex location would be observed.

Figure 7a shows the variation of the trailing-edge pressures along the span of the flap, and Fig. 7b shows the corresponding integrated flap lift coefficient. The general trailing-edge pressure decreases with increasing h_G and is consistent with 2-D studies on two-element airfoils [42]. The significant decrease in pressure toward the flap edge (Fig. 7a), together with the sharp change in slope of the flap lift (Fig. 7b), is typical of the pressure signature generated by a vortex that is partially rolled up on a flap surface or square wingtip [43,44]. The similar form of all pressure distributions is an indication that the vortex rolls up partially on the flap edge both for the baseline case and for the Gurney flap cases.

VII. Wing Load Variations

To quantify the changes in lift C_L and drag C_D coefficients for different Gurney flap configurations, load measurements were performed using the six-component balance described in Sec. IV. Aerodynamic coefficients are based on the geometry of the unflapped wing (see Vey et al. [38]) and some representative data are shown in Figs. 8a–8d. The principle errors in the measurement of aerodynamic coefficients were those due to the balance nonlinearity. Based on maximum errors of 0.23% in both the lift and drag force measurements (see discussion in Sec. IV), error bands are too small to practically represent on the figure and are typically on the order of the symbol sizes in Figs. 8a–8d.

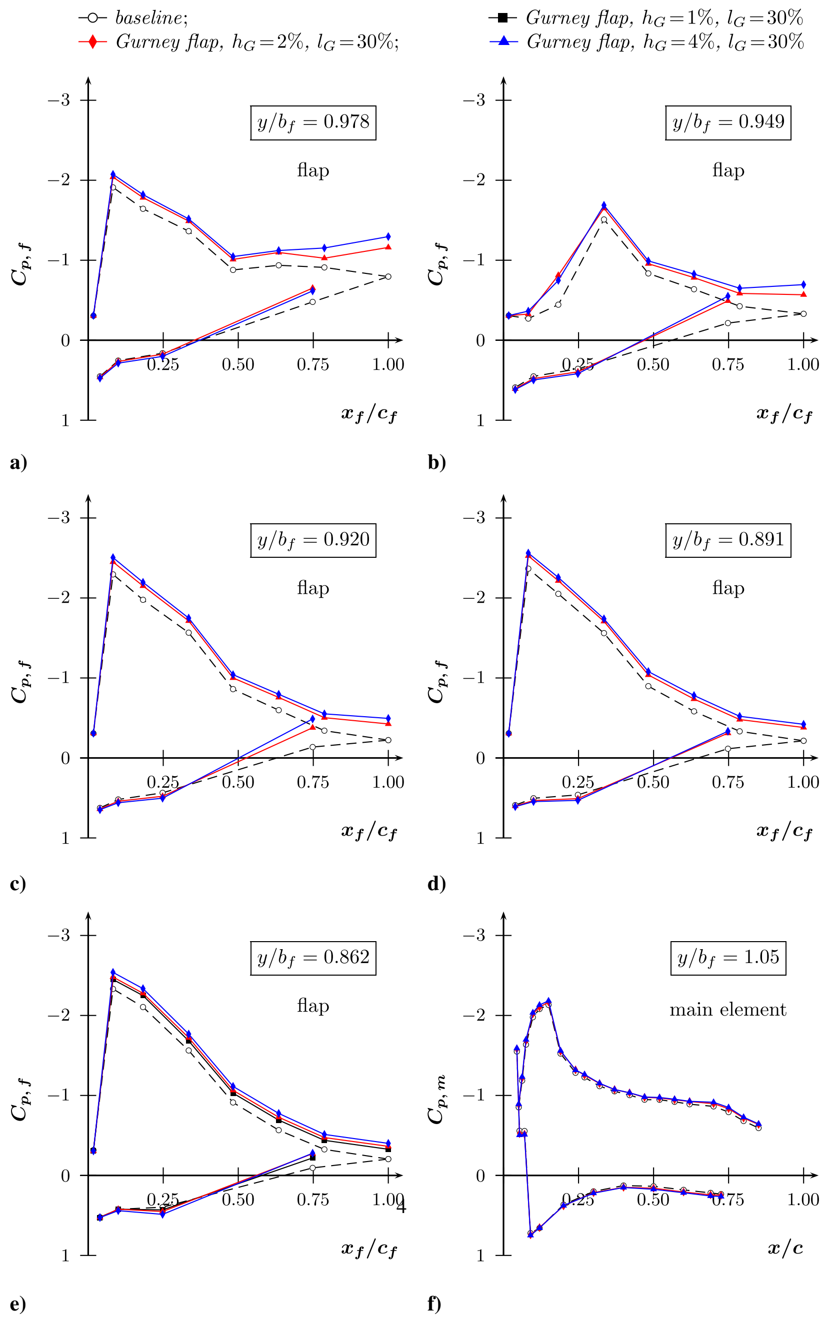

Fig. 6 Pressure coefficient distributions in the vicinity of the flap edge and on the wing main element.

At all prestall angles of attack, the lift coefficient is slightly larger with the Gurney flaps installed (Fig. 8b). Increasing both Gurney flap height and length has the effect of further increasing lift. However, due to the small faction of the span covered by the Gurney flaps, the changes to the aerodynamic indicators are relatively small: changes in C_L and C_D are summarized in Table 1 for an angle of attack $\alpha = 5$ deg at $Re = 500,000$. For example, with $l_G = 30$ and 40%, the fractions of the half-wing that incorporate the Gurney flaps are 15 and 20%, respectively. Consequently, for a relatively large flap height ($h_G = 4\%$ and $l_G = 30\%$) the overall change in the half-wing lift is only 6% (see Table 1). This is much smaller than if the entire half-wing would have been equipped with a Gurney flap (e.g., Liu and Montefort [45]). Consistent with this, the dependence of C_L on both Gurney flap height and length is weak. For example, with $l_G = 30\%$ at $\alpha = 5$ deg, an increase in flap height by from 2 to 4% produces a change in C_L of less than 0.01.

It can be seen from Figs. 8c and 8d that drag increases slightly and, consequently, the aerodynamic efficiency C_L/C_D decreases when Gurney flaps are installed, but these changes are relatively small with the wing in landing configuration (see inset). Once again, the small changes are due to the relatively small span that the Gurney flaps occupy. However, to address the problem of increasing drag, three-dimensionality can be added to the Gurney flaps by means of slits or holes (see Meyer et al. [37]). The introduction of the three-dimensionality suppresses vortex-shedding, thereby reducing drag. Nevertheless, changes to C_L are not materially affected by the three-dimensionality and this produces an increase in efficiency.

In light of the fact that there is no theoretical means of predicting how much centroidal shift is considered satisfactory and necessary to significantly hasten linking and mutual destruction of the vortices, the present data have been compared with towing-tank data of Crouch et al. [22]. On a flaps-down configuration, they showed that periodic perturbations produced early linking of the trailing vortices. The vortex perturbation amplitude was quantified as a peak-to-peak lift fluctuation $\Delta C_L/C_L$ (namely, the lift that is shifted between inboard and outboard stations ΔC_L) normalized by the total wing lift

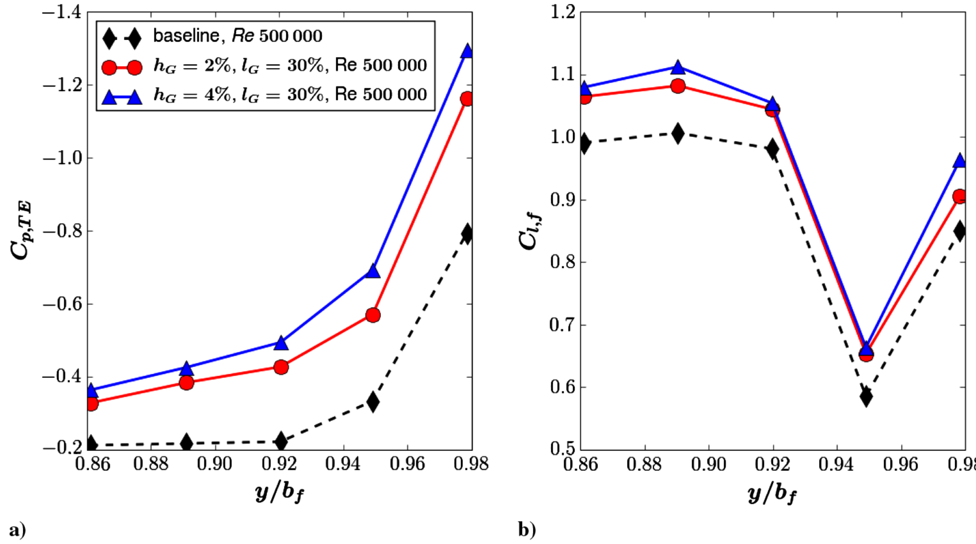

Fig. 7 Spanwise variation of the a) pressure coefficient along the flap's trailing edge and b) local sectional lift coefficient along flap span near the outboard edge.

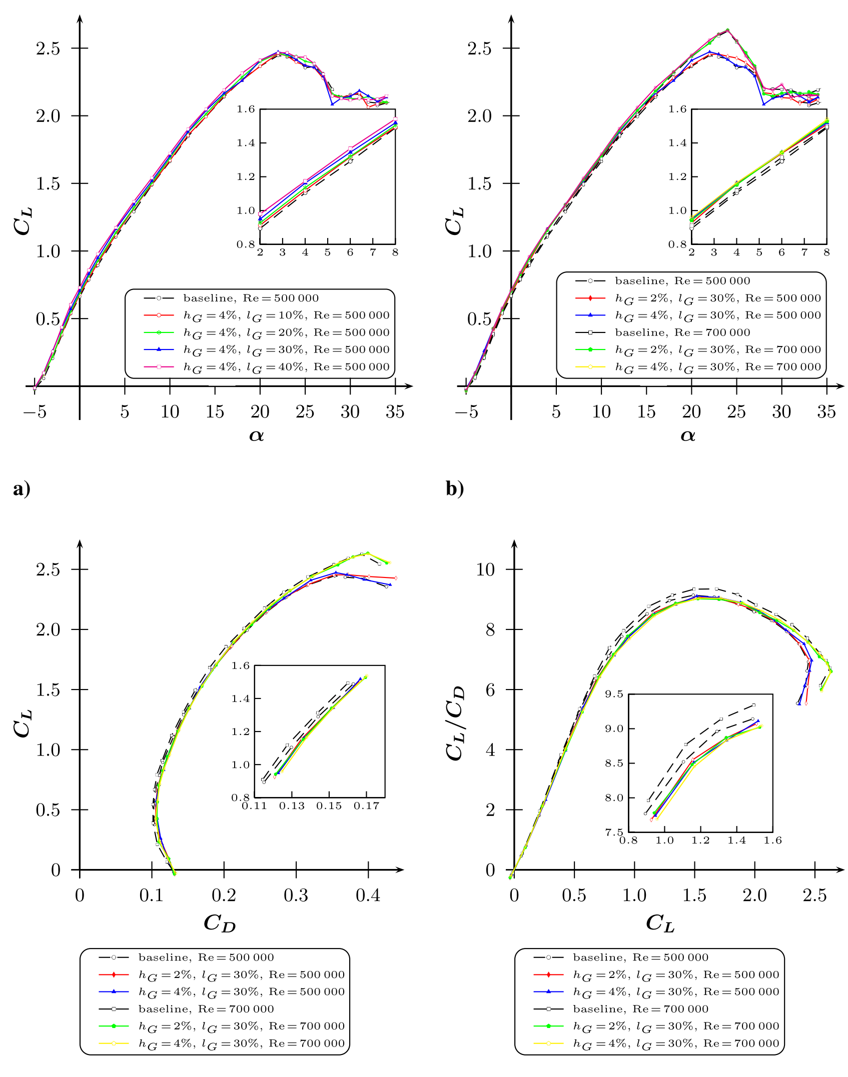

Fig. 8 Influence of Gurney flaps on aerodynamic loads: a) C_L vs α for varying Gurney flap length, b) C_L vs α for varying Gurney flap height, c) C_L vs C_D (same configurations as in b), and d) aerodynamic efficiency C_L/C_D vs C_L. The same Gurney flap configurations are in b, c, and d; $Re = 500,000$ and 700,000.

Table 1 Changes in C_L and C_D at $\alpha = 5$ deg for different Gurney flap configurations, based on direct load measurements at $Re = 500,000$

	$h_G = 2\%, l_G = 30\%$	$h_G = 2\%, l_G = 40\%$	$h_G = 4\%, l_G = 30\%$	$h_G = 4\%, l_G = 40\%$
ΔC_L	0.0495	0.0533	0.0557	0.0722
$\Delta C_L/C_L$	4.13%	4.45%	4.65%	6.03%
ΔC_D	0.0063	0.0085	0.0075	0.0163
$\Delta(C_L/C_D)$	−0.46%	−1.83%	−0.91%	−5.37%

C_L. In their towing-tank study, perturbations were achieved by periodically cycling the inboard and outboard control surfaces, designed to introduce spatially periodic perturbations to the wingtip and inboard flap-edge vortex positions. The fastest linking of vortices was achieved with $\Delta C_L/C_L = 6\%$.

In the present investigation, the fluctuations in lift ($\Delta C_L/C_L$) for various Gurney flap configurations are between 4 and 6% (Table 1). Thus, despite the relatively small lift fluctuation, it can be inferred that a single larger Gurney flap can produce sufficient lift fluctuations to produce rapid linking of the vortices. Furthermore, the peak-to-peak lift fluctuations cited by Crouch et al. [22] are based on the deflection of two (sets of) control surfaces. Consequently, to present an appropriate comparison, consider a second Gurney flap placed at the inboard edge of the flap. If the inboard and flap-edge flaps were then deployed alternately, out of phase, the peak-to-peak lift fluctuations cited in Table 1 would have to be doubled to between 8 and 12%. It can thus clearly be seen that the required peak-to-peak fluctuations could easily be achieved and even exceeded using additional Gurney flaps.

VIII. Dynamic Vortex Measurements

PIV measurements were made in the wake aft of the flap edge while driving the Gurney flap using the pushrod and cam mechanism described in Sec. IV. Data were acquired at eight equal phases of the motor rotation Φ. Two Gurney flap configurations were considered for the dynamic measurements: namely, $h_G = 2$ and 4%, both with a length of $l_G = 30\%$. The $l_G = 30\%$ configurations were chosen for active Gurney flap tests based on the trends shown in Fig. 5. Various forcing frequencies were tested, corresponding to perturbation wavelengths listed in Table 2. The Gurney flap deflection angle δ_G can be related to the phase angle Φ according to

$$\delta_G = 90\,\text{deg} \times \sin(\Phi/2); \qquad 0\,\text{deg} \leq \Phi \leq 360\,\text{deg} \tag{3}$$

and this is shown schematically in Fig. 9. The PIV data were processed and plotted as a function of the Gurney flap phase angle (Figs. 10–13); hence, the PIV realizations do not coincide directly with this angle. The corresponding phase shifts ΔΦ required for directly corresponding measurements, however, were estimated

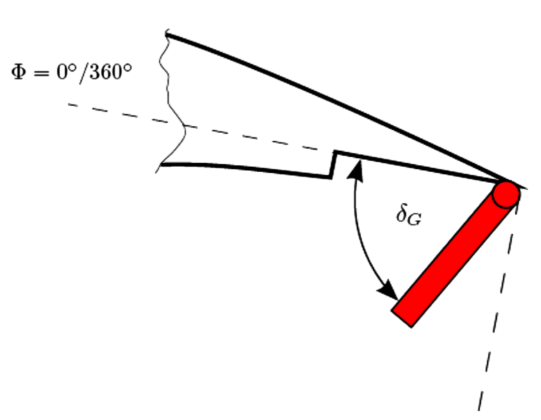

Fig. 9 Relation between phase angle Φ and Gurney flap deflection angle δ_G.

Table 2 Forcing frequencies, corresponding wavelengths, and phase shift considered at a velocity of $U_\infty = 16.2$ m/s

f	2.5 Hz	5.0 Hz	10 Hz
λ/b	2.89	1.45	0.72
$\Delta\Phi$ ($x/c = 4$)	75 deg	150 deg	300 deg
$\Delta\Phi$ ($x/c = 9$	214.7 deg	69.4 deg	138.9 deg

based on the Gurney flap oscillatory frequency and freestream velocity and are listed in Table 2. It is pointed out, however, that this phase shift has no bearing on the major conclusions presented below.

The wavelength of the most unstable mode of the Crow instability for the flap vortices is $\lambda \approx 9b_0$, where b_0 is the initial separation distance of the rolled-up vortices. At $Re = 500,000$, corresponding to a freestream velocity of $U_\infty = 16.2$ m/s, the resulting forcing frequency is $f = U_\infty/(9b_0) = 1.61$ Hz. At these low frequencies, the electric motor used to drive the cam rotated nonuniformly, and hence high-fidelity phase-locked vortex measurements could not be made. Consequently, the frequencies considered here are higher, corresponding to shorter, faster-growing wavelength instabilities typical of the Crouch instability. The difference between Crow [46] and Crouch instabilities is discussed in Crouch et al. [22]. Essentially, the Crouch instability leaves the vorticity centroid of the wing unperturbed, whereas, to excite the Crow instability, the vorticity centroid is perturbed. With active Gurney flaps deployed on both inboard and outboard edges of the flap, both scenarios are realizable [30,31]. Detailed measurements were undertaken for the $f = 2.5$, 5, and 10 Hz cases ($\lambda/b = 2.89$, 1.45, and 0.72), where the PIV system was triggered at eight phases. The vortex centroid trajectories are plotted as a function of Gurney flap phase (0 deg ≤ ΔΦ ≤ 360 deg) for all the dynamic cases in Figs. 10–13. The peak vorticity $\omega_{x,\max}$ is shaded in the plots to reflect the local changes in aerodynamic loads (i.e., changes in shed vorticity as the Gurney flap oscillates through the cycle). Mutually perpendicular centroid shifts in y and z directions were projected onto the corresponding axes and the static centroid locations were indicated for comparison. The open symbols in all figures indicate the baseline centroid. The projections show that the dynamic vortices behave in a qualitatively similar manner to their static counterparts. Namely, lateral vortex displacement increases with downstream distance, but longitudinal displacement reduces. A numerical comparison of centroid displacements is summarized in Table 3, which emphasizes this observation. At $x/c = 4$ centroid perturbations obtained by means of dynamic Gurney flaps are larger than in the static case. In the case of the $x/c = 9$ position, this holds true for the z direction only, $\Delta\bar{y}$ being on the order of the static case. There is no clear dependence of perturbation amplitude on forcing frequency. Therefore, it can be concluded that perturbing the vortices at frequencies that correspond to wavelengths in the range $0.72 \leq \lambda/b \leq 2.89$ does not materially affect the vortex centroid control authority. No attempt was made in this investigation to determine the minimum wavelength for which this remains true.

A further observation that can be made from Figs. 10–13 is that the Gurney flap oscillation frequency becomes more pronounced with downstream distance. This is particularly evident when comparing high-frequency (short-wavelength) perturbations. Close to the flap ($x/c = 4$; Fig. 13a) there is no clear perturbation wavelength evident from the y-axis projection. Further downstream, however ($x/c = 9$; Figs. 13b), the corresponding perturbation

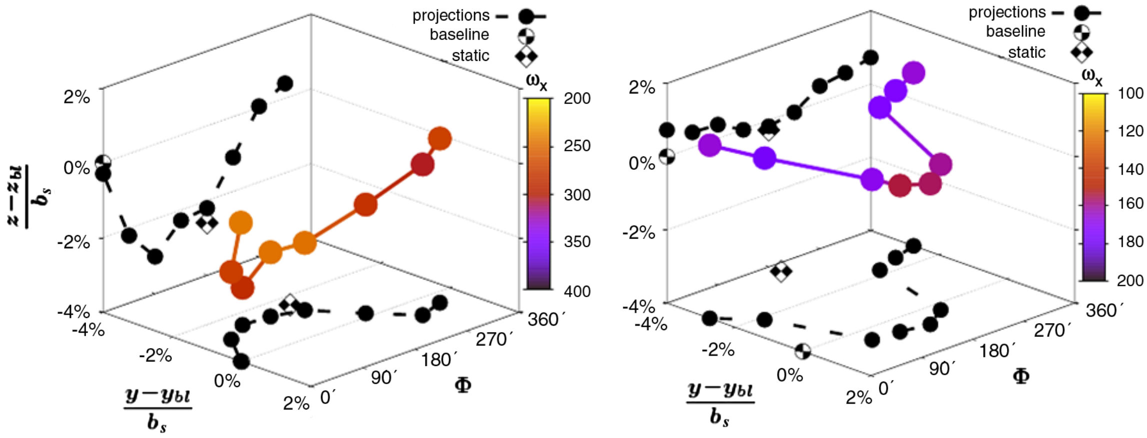

a) b)

Fig. 10 Vortex trajectories as a function of phase for $h_G = 2\%, f = 2.5$ Hz, and $\lambda/b = 2.89$ at a) $x/c = 4$ and b) $x/c = 9$.

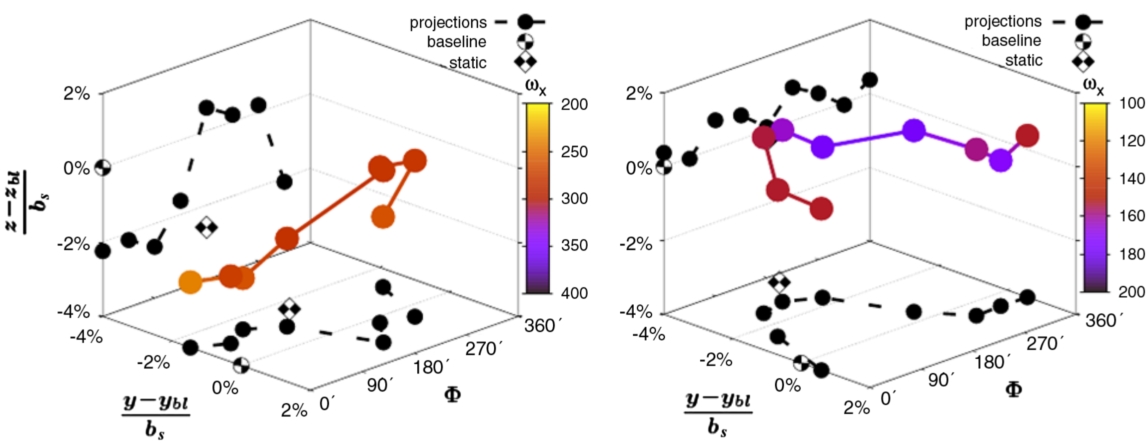

a) b)

Fig. 11 Vortex trajectories as a function of phase for $h_G = 2\%, f = 5$ Hz, and $\lambda/b = 1.45$ at a) $x/c = 4$ and b) $x/c = 9$.

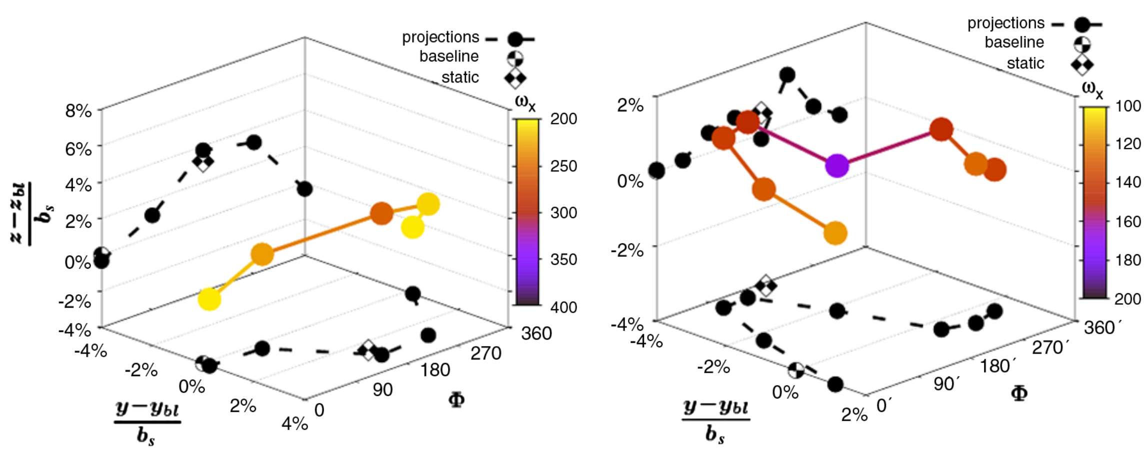

a) b)

Fig. 12 Vortex trajectories as a function of phase for $h_G = 4\%, f = 5$ Hz, and $\lambda/b = 1.45$ at a) $x/c = 4$ and b) $x/c = 9$.

wavelength is clearly evident. The reason for this is not clear; however, as the vortex moves downstream it is composed of a greater fraction of the vortex sheet, which is distorted at the flap edge. The rolling-up process may introduce perturbations that distort the vortex and cause it to meander. With more of the vortex sheet rolled up, the effect of the distortions reduces and the input frequency is more clearly evident.

A surprising observation that was made for static and dynamic cases, including all baseline and control cases, was that the flap-edge vortex strength decreased in the downstream direction. The tip vortex strength, on the other hand, did not diminish as far downstream as $x/c = 22$ ($x/b = 4.5$). In fact, for $x/c > 9$ the flap-edge vortex strength dropped dramatically and could not be detected with a matrix of tufts. Additionally, smoke introduced from the edge of the

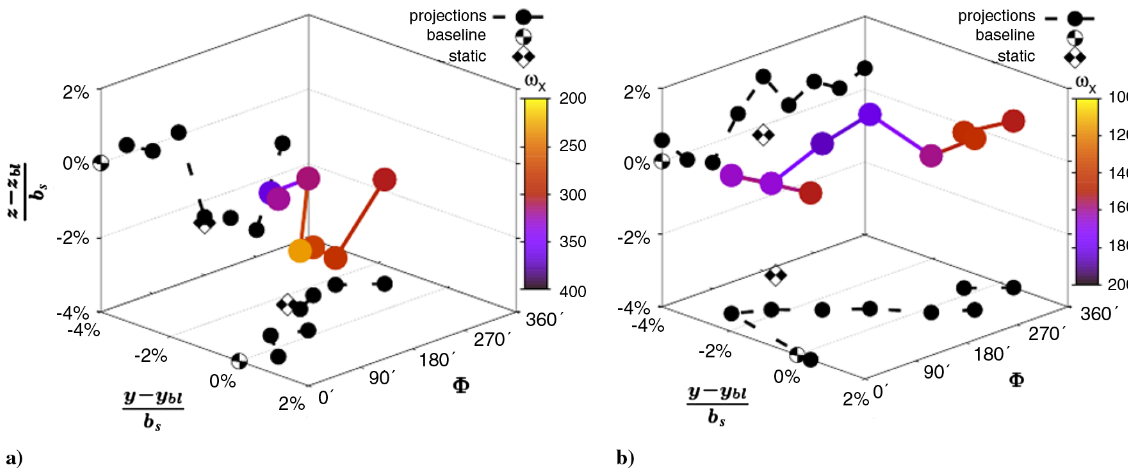

Fig. 13 Vortex trajectories as a function of phase for $h_G = 2\%$, $f = 10$ Hz, and $\lambda/b = 0.72$ at a) $x/c = 4$ and b) $x/c = 9$.

flap indicated what appeared to be vortex breakdown at approximately $x/c = 15$, although this was not verified by measurements; retrospectively, a simple total head probe could have been used to establish the existence of a stagnation point. This observation was counterintuitive and not in keeping with data acquired on wind-tunnel models and full-scale airliners; vortex strength generally increases as more of the shed vorticity is rolled up. The main reason for vortex breakdown appeared to be the combination of large flap deflection (32 deg) together with a highly swept trailing edge ($\Lambda = 30$ deg). Vortex breakdown has been observed on unswept flap edges with very large angles of attack and flap deflections [47], but this usually occurs in the vicinity of the flap edge and not several chord lengths downstream, as in the present case. In this regard, it is important to note that the present model does not have the planform of a conventional airliner. Rather, both the leading and trailing edges are swept at a constant 30 deg along the entire span. The original design incorporated a full-span flap; this was shortened here for the express purpose of the present study. This unique setup may serve as a vehicle for studying the enigmatic vortex breakdown or bursting phenomena.

Table 3 Centroid excursions when employing the active Gurney flap at different wavelengths with $l_G = 30\%$

		$x/c = 4$		$x/c = 9$	
f, Hz	λ/b	$\Delta\bar{y}/b_s$	$\Delta\bar{z}/b_s$	$\Delta\bar{y}/b_s$	$\Delta\bar{z}/b_s$
		$h_G = 2\%$			
Static	∞	1.61	2.59	3.64	0.26
2.5	2.89	2.20	3.40	3.49	0.89
5.0	1.45	2.58	3.24	3.40	0.97
10.0	0.72	2.10	3.52	3.44	1.87
		$h_G = 4\%$			
5.0	1.45	2.50	3.15	3.86	0.57

IX. Comparison of Different Methods

In this section the present data are compared to the vortex centroid results of other research known to the authors. To account for the different-aspect-ratio semispan wings (AR_s) used in the various investigations, the maximum attained perturbation of the vortex centroids is presented in terms of $\Delta\bar{y}/b_s$ as well as $\Delta\bar{y}/b_s \times AR_s$; the latter term is equivalent to $\Delta\bar{y}/\bar{c}$, where $\bar{c}$ is the mean chord length. The data presented in Table 4 were taken in the near field of the wake at various comparable downstream positions. An ideal comparison would require different control mechanisms to be applied to one and the same model, with measurements at the same downstream location under identical conditions. Nevertheless, the comparison presented here provides insight into the various techniques and their application to different aspects of the wing.

Table 4 Comparison of maximum lateral centroid perturbation for different investigations

Wing/profile type	Investigation type	$\Delta\bar{y}/b_s$	$\Delta\bar{y}/b_s \times AR_s$	Re	Measured x/c
	Matalanis and Eaton [27,28]				
NACA 0012	Gurney Flaps of $h_G = 1.5\%$ at the wingtip	2.05%	4.10%	350,000	4.9
	Coustols [26]				
Very large transport aircraft half-model	Continuous and pulsed blowing at the wing tip	~0.42%	~1.9%	450,000 to 750,000	1
	Greenblatt [30,31]				
NACA 0015 with inboard flap deflection	Passive and active flap separation control	2.70%	5.4%	500,000 to 10^6	2
	Greenblatt et al. [32]				
NACA 0015 with tip flap deflection	Active wingtip separation control	1.4% 2.2%	2.8% 4.4%	500,000 to 10^6	2.2 7.2
	Present				
SCCH	Gurney flap $h_G = 2\%$, $l_G = 30\%$ at the flap edge	2.58%	6.42%	500,000 to 700,000	4
SCCH	Gurney flap $h_G = 4\%$, $l_G = 30\%$ at the flap edge	2.8%	6.94%	500,000 to 700,000	4
SCCH	Gurney flap $h_G = 2\%$, $l_G = 40\%$ at the flap edge	4.10%	10.17%	500,000 to 700,000	9
SCCH	Gurney flap $h_G = 4\%$, $l_G = 40\%$ at the flap edge	5.30%	13.14%	500,000 to 700,000	9

Wing tip vortex control by static Gurney flaps was addressed by Matalanis and Eaton [27]. They equipped the wing of a half-span model with so-called miniature trailing-edge effectors (MiTEs), that are essentially a novel active Gurney flap arrangement of $h_G = 1.5\%$. Their experiments were conducted on a semispan NACA 0012 (AR $= 4.1$) at $\alpha = 8.9$ deg and $Re = 350,000$. The wing composed of Gurney flaps deployed on large fractions of span were found to predominately control the vortex in the direction of lift (vertical direction), whereas Gurney flaps deployed over a small fraction of the span shifted the vortex both in spanwise and vertical directions. This observation is fully consistent with Betz's [36] hypothesis. In the Matalanis and Eaton [27] study, the measurement plane was placed at $x/c = 4.9$ downstream of the wing. They also concluded that actively deployable MiTEs may be used for wake alleviation. In a more recent paper by the same authors (Matalanis and Eaton [28]), the tip vortex of the same model was controlled by rapidly actuated Gurney flaps. Computational simulations by the authors showed that MiTEs are capable of exciting instabilities in four vortex configurations, thus concluding that a reduction in aircraft spacing rules would be possible. The effect of Gurney flaps on wing tip vortices was also addressed by Nikolic [29], who found that the addition of Gurney flaps alters the near-field roll-up pattern of a wing tip vortex. He visualized the vortex structure with tufts and found that tip vortex strength decreased with increasing Gurney flap height. This is in contrast to theory, because Gurney flaps increase the local circulation, and therefore vortex strength should be increasing with growing Gurney flap height. The apparent reduction in vortex strength was probably due to the wake shed by the Gurney flaps [37], which is rolled up into the vortex, rendering it more diffuse.

Finally, Coustols et al. [26] of ONERA influenced the wing tip vortex of a very large transport aircraft half-model at $450,000 \leq Re \leq 750,000$ by continuous and pulsed blowing at the wing tip. Their work was also aimed at exciting instabilities in the trailing vortex system. Apart from active control techniques, Coustols et al. investigated differential flap settings to create a multiple-vortex system with enhanced decay characteristics.

It is evident from Table 4 that, in general, control at the flap edge produces larger vortex perturbations than control at the wingtip. Based on the Donaldson–Betz hypothesis, the main reason for this is because the vortex rolls up from $|d\Gamma/dy|_{\max}$; in the case of the wingtip, this is theoretically at $y = b_s$, where $d\Gamma/dy \to \infty$; in the case of the flap-edge region, this is at the span-loading inflection point and is theoretically finite. Thus, it is much more difficult to perturb the wingtip vortex theoretically, as small changes to large $d\Gamma/dy$ will not produce a strong effect (e.g., [26,32]). In contrast, in the vicinity of the flap edges, $|d\Gamma/dy|_{\max}$ is finite and this finite peak can readily be displaced along the span in order to perturb the vortex in the spanwise direction. This is seen by comparing separation control on inboard and tip flaps (cf. [31] versus [32]) at $x/c \approx 2$, where the perturbation is nearly twice as large in the former case. A similar conclusion can be drawn by comparing Matalanis and Eaton [27,28] and the present study. More evidence for this hypothesis is provided by jet blowing into the vortex core, which does not fundamentally alter the span-loading (i.e., the vortex-sheet from which the vortex rolls up). This might be the reason for the small centroid shifts compared to the other techniques.

The data of the present investigation together with those of Matalanis and Eaton [27,28] and Nikolic [29] clearly show the utility of Gurney flaps for wake vortex management and, potentially, for vortex alleviation. To the best knowledge of the authors of this paper, however, the effect of Gurney flaps on far-field vortex development has not been evaluated experimentally. Furthermore, the technique has not been assessed in flight tests. Nevertheless, there are platforms with the potential to test the method [39] in which deployable Gurney flaps can be employed on the flaps.

X. Conclusions

Based on a pilot study conducted at NASA Langley Research Center, the present follow-up investigation at the Technical University of Berlin in collaboration with the DLR, German Aerospace Center has demonstrated the basic mechanism for managing trailing vortices using retrofitted devices that are decoupled from the conventional control surfaces. The premise for managing vortices is rooted in the method of Betz [36], as extended to flaps by Donaldson et al. [35]. Using various devices, vortices may be perturbed at arbitrarily long wavelengths down to wavelengths less than a typical airliner wingspan without loss of vortex authority. Moreover, balance-measured oscillatory loads on the wings, and hence the projected aircraft, are small. Significant flexibility in the specific device has been demonstrated using local passive and active separation control as well as local circulation control via Gurney flaps. Clearly, a combination of devices can be used, such as vortex generators and Gurney flaps: the former are used on conventional high-lift systems (e.g., Nield [48]) and the latter on experimental aircraft (e.g., Hansen [39]). For application to a wake vortex alleviation scheme, these traditionally passive devices must be driven in a time-dependent manner.

The method is now in a position to be tested in a wind tunnel with a longer test section on a scaled airliner configuration. Alternatively, the method can be tested directly in a towing tank, on a model aircraft, on a light aircraft, or on a full-scale airliner. The authors believe that this method will have significant appeal from an industry perspective, due to its retrofit potential with little-to-no impact on cruise (devices tucked away in the cove or retracted), low operating power requirements, small lift oscillations when deployed in a dynamic manner, and significant flexibility with respect to the specific devices selected.

Acknowledgments

The authors would like to like to acknowledge the support and assistance of H. Stolpe, R. Nagel, and W. Hage. Permission to use the photographs was kindly provided by Jan-Olov Newborg, Chris Haag, Andreas Stoeckl, and Ryan Hemmings.

References

[1] Spalart, P. R., "Airplane Trailing Vortices," *Annual Review of Fluid Mechanics*, Vol. 30, 1998, pp. 107–138. doi:10.1146/annurev.fluid.30.1.107

[2] Rossow V. J., "Lift-Generated Vortex Wakes of Subsonic Transport Aircraft," *Progress in Aerospace Sciences*, Vol. 35, No. 6, 1999, pp. 507–660. doi:10.1016/S0376-0421(99)00006-8

[3] "Wake Turbulence: An Obstacle to Increased Air Traffic Capacity," The National Academies Press, Washington, D.C., 2008, www.nap.edu/catalog/12044.html [retrieved April 2008].

[4] Kingsley-Jones, M., "Boeing 747-8 vs A380: A Titanic Tussle," Feb. 2006, http://www.flightglobal.com/articles/2006/02/17/205137/boeings-747-8-vs-a380-a-titanic-tussle.html [retrieved April 2008]

[5] Savaş, Ö., "Experimental Investigations on Wake Vortices and Their Alleviation," *Comptes Rendus Physique*, Vol. 6, Nos. 4–5, 2005, pp. 415–429. doi:10.1016/j.crhy.2005.05.004

[6] Crouch, J. D., "Airplane Trailing Vortices and Their Control," *Comptes Rendus Physique*, Vol. 6, Nos. 4–5, 2005, pp. 487–499. doi:10.1016/j.crhy.2005.05.006

[7] Michel, U., and Böhning, P., "Investigation of Aircraft Wake Vortices with Phase Microphone Arrays," AIAA Paper 2002-2501, 2002.

[8] Schmitt, N. P., Rehm, W., Pistner, T., Zeller, P., Diehl, H., and Navé, P., "The AWIATOR Airborne LIDAR Turbulence Sensor," *Aerospace Science and Technology*, Vol. 11, Nos. 7–8, 2007, pp. 546–552. doi:10.1016/j.ast.2007.03.006

[9] Fine, N. E., and Kring, D. C., "Opto-Acoustic Tracking of Aircraft Wake Vortices," 11th AIAA/CEAS Aeroacoustics Conference, 26th AIAA Aeroacoustics Conference, AIAA Paper 2005-2965, Monterey, CA, May 2005.

[10] Frech, M., and Holzäpfel, F., "Skill of an Aircraft Wake-Vortex Model Using Weather Prediction and Observation," *Journal of Aircraft*, Vol. 45, No. 2, March–April 2008, pp. 461–470. doi:10.2514/1.28983

[11] Rennich, S. C., and Lele, S. K., "Method for Accelerating the Destruction of Aircraft Wake Vortices," *Journal of Aircraft*, Vol. 36, No. 2, 1999, pp. 398–404. doi:10.2514/2.2444

[12] Rossow, V. J., "Theoretical Study of Lift-Generated Vortex Wakes Designed to Avoid Rollup," *AIAA Journal*, Vol. 13, No. 4, 1975, pp. 476–484.
doi:10.2514/3.49734

[13] Cliffone, D. L., and Orloff, K. L., "Far Field Wake-Vortex Characteristics of Wings," *Journal of Aircraft*, Vol. 12, No. 5, 1975, pp. 464–470.
doi:10.2514/3.59825

[14] Ortega, J. M., Bristol, R. L., and Savaş, Ö., "Experimental Study of the Instability of Unequal-Strength Counter-Rotating Vortex Pairs," *Journal of Fluid Mechanics*, Vol. 474, 2003, pp. 35–84.
doi:10.1017/S0022112002002446

[15] Fabre, D., Jacquin, L., and Loof. A., "Optimal Perturbations in a Four-Vortex Aircraft Wake in Counterrotating Configuration," *Journal of Fluid Mechanics*, Vol. 451, 2002, pp. 319–328.
doi:10.1017/S0022112001006954

[16] Durston, D. A., Walker, S. M., Driver, D. M., Smith, S. C., and Savaş, Ö., "Wake-Vortex Alleviation Flowfield Studies," *Journal of Aircraft*, Vol. 42, No. 4, 2005, pp. 894–907.
doi:10.2514/1.7904

[17] Chevalier, H., "Flight Test Studies of the Formation and Dissipation of Trailing Vortices," *Journal of Aircraft*, Vol. 10, No. 1, 1973, pp. 14–18.
doi:10.2514/3.60193

[18] Crow, S. C., "Panel Discussion," *Aircraft Wake Turbulence and Its Detection*, edited by J. H. Olsen, A. Goldburg, and M. Rogers, Plenum, New York, 1971, pp. 580–582.

[19] Crow, S. C., and Bate, E. R., "Lifespan of Trailing Vortices in a Turbulent Atmosphere," *Journal of Aircraft*, Vol. 13, No. 7, 1976, pp. 476–482.
doi:10.2514/3.44537

[20] Haverkamp, S., Neuwerth, G., and Jacob, D., "Active and Passive Vortex Wake Mitigation Using Control Surfaces," *Aerospace Science and Technology*, Vol. 9, No. 1, Jan. 2005, pp. 5–18.
doi:10.1016/j.ast.2004.08.005

[21] Bilanin, A. J., and Widnall, S. E., "Aircraft Wake Dissipation by Sinusoidal Instability and Vortex Breakdown," AIAA Paper 73-107, 1973.

[22] Crouch, J. D., Miller, G. D., and Spalart, P. R., "Active-Control System for Breakup of Airplane Trailing Vortices," *AIAA Journal*, Vol. 39, No. 12, 2001, pp. 2374–2381.
doi:10.2514/2.1244

[23] Pradeep, D. S., and Hussain, F., "Transient Growth of Perturbations in a Vortex Column," *Journal of Fluid Mechanics*, Vol. 550, No. -1, 2006, pp. 251–288.
doi:10.1017/S0022112005008207

[24] Brion, V. D., Sipp, and Jacquin, L., "Optimal Amplification of the Crow Instability," *Physics of Fluids*, Vol. 19, 2007, Paper. 111703.
doi:10.1063/1.2793146

[25] Crouch, J. D., "Forcing the Breakup of Airplane Trailing Vortices," *Conference on Capacity and Wake Vortices*, Imperial College of Science, Technology and Medicine, London, Sept. 2001.

[26] Coustols, E., Jacquin, L., Moens, F., and Molton, P., "Status of ONERA Research on Wake Vortex in the Framework of National Activities and European Collaboration," *European Congress on Computational Methods in Applied Sciences and Engineering (ECCOMAS)*, 2004, http://www-mip.onera.fr/projets/WakeNet2-Europe/fichiers/publications/publi2004/ECCOMAS2004_STS15_Coustols_et_al.pdf [retrieved April 2008].

[27] Matalanis, C. G., and Eaton, J. K., "Wake Vortex Control Using Static Segmented Gurney Flaps," *AIAA Journal*, Vol. 45, No. 2, 2007, pp. 321–328.
doi:10.2514/1.25956

[28] Matalanis, C. G., and Eaton, J. K., "Wake Vortex Alleviation Using Rapidly Actuated Segmented Gurney Flaps," *AIAA Journal*, Vol. 45, No. 8, 2007, pp. 1874–1884.
doi:10.2514/1.28319

[29] Nikolic, V. R., "Effect of Full-Span Gurney Flap Height on Wing Wake Vortex Alleviation," *Journal of Aircraft*, Vol. 43, No. 5, 2006, pp. 1555–1558.
doi:10.2514/1.19369

[30] Greenblatt, D., "Management of Vortices Tailing Flapped Wings via Separation Control," 43rd AIAA Aerospace Sciences Meeting and Exhibit, AIAA Paper 2005-0061, Reno, Jan. 2005.

[31] Greenblatt, D., "Managing Flap Vortices via Separation Control," *AIAA Journal*, Vol. 44, No. 11, 2006, pp. 2755–2764.
doi:10.2514/1.19664

[32] Greenblatt, D., Melton, L., Yao, C., and Harris, J., "Control of a Wing Tip Vortex," 23rd AIAA Applied Aerodynamics Conference, AIAA Paper 2005-4851, Toronto, June 2005.

[33] de Bruin, A. C., Hegen, S. H., Rohne, P. B., and Spalart, P. R., "Flow Field Survey in the Trailing Vortex System Behind a Civil Aircraft Model at High Lift," AGARD CP-584, Neuilly-sur-Seine, France, 1996, pp. 25-1–25.12.

[34] Bellastrada, C., Breitsamter, C., and Laschka, B., "Investigation of Turbulent Wake Vortex Originating From a Large Transport Aircraft in Landing Configuration," *Proceedings of the CEAS Aerospace Aerodynamics Research Conference*, 2002, pp. 31.1–31.10.

[35] Donaldson, C. D., Snedeker, R. S., and Sullivan, R. D., "Calculation of Aircraft Wake Velocity Profiles and Comparison with Experimental Measurements," *Journal of Aircraft*, Vol. 11, No. 9, 1974, pp. 547–555.
doi:10.2514/3.60385

[36] Betz, A., "Behavior of Vortex Systems," *Zeitschrift für Angewandte Mathematik und Mechanik*, Vol. 12, No. 3, June 1932, pp. 164–174.
doi:10.1002/zamm.19320120307

[37] Meyer, R., Hage, W., Bechert, D. W., Schatz, M., and Thiele, F., "Drag Reduction on Gurney Flaps by Three-Dimensional Modifications," *Journal of Aircraft*, Vol. 43, No. 1, 2006, pp. 132–140.
doi:10.2514/1.14294

[38] Vey, S., Greenblatt, D., Paschereit, C. O., and Meyer, R., "Flap Vortex Management by Active Gurney Flaps," 46th AIAA Aerospace Sciences Meeting and Exhibit, Reno, NV, AIAA Paper 2008-286, Jan. 2008.

[39] Hansen, H., "Application of Mini-Trailing-Edge Devices in the AWIATOR Project," Airbus Deutschland, Bremen, Germany, 2003, http://www.kat-net.net/news/display.php?id=110 [retrieved Oct. 2009].

[40] Li, Y., Wang, J., and Zhang, P., "Influences of Mounting Angles and Locations on the Effects of Gurney Flaps," *Journal of Aircraft*, Vol. 40, No. 3, 2003, pp. 494–498.
doi:10.2514/2.3144

[41] Jeffrey, D., Zhang, X., and Hurst, D. W., "Aerodynamics of Gurney Flaps on a Double-Element Wing," *Journal of Fluids Engineering*, Vol. 123, No. 1, 2001, pp. 99–104.
doi:10.1115/1.1334376

[42] Jeffrey, D., Zhang, X., and Hurst, D. W., "Aerodynamics of Gurney Flaps on a Single-Element High-Lift Wing," *Journal of Aircraft*, Vol. 37, No. 2, 2000, pp. 295–301.
doi:10.2514/2.2593

[43] McAlister, K. W., and Takahashi, R. K., "NASA 0015 Wing Pressure and Trailing Vortex Measurements," NASA TP 3151 Nov. 1991.

[44] Greenblatt, D., and Washburn, A. E., "Influence of Finite Span and Sweep on Active Flow Control Efficacy," *AIAA Journal*, Vol. 46, No. 7, 2008, pp. 1675–1694.
doi:10.2514/1.33809

[45] Liu, T., and Montefort, J., "Thin-Airfoil Theoretical Interpretation for Gurney Flap Lift Enhancement," *Journal of Aircraft*, Vol. 44, No. 2, 2007, pp. 667–671.
doi:10.2514/1.27680

[46] Crow, S., "Stability Theory for a Pair of Trailing Vortices," *AIAA Journal*, Vol. 8, 1970, pp. 2172–2179.
doi:10.2514/3.6083

[47] Radeztsky, R. H., Jr., Singer, B. A., and Khorrami, M. R., "Detailed Measurements of a Flap Side-Edge Flow Field," 36th AIAA Aerospace Sciences Meeting and Exhibit, Reno, NV, AIAA Paper 1998-700, Jan. 1998.

[48] Nield, B. N., "An Overview of the Boeing 777 High-Lift Aerodynamic Design," *The Aeronautical Journal*, Vol. 99, Nov. 1995. pp. 361–371.

N. Chokani
Associate Editor